

Detonation propagation in annular arcs of condensed phase explosives

Eleftherios Ioannou,^{a)} Stefan Schoch, Nikolaos Nikiforakis, and Louisa Michael
*Laboratory for Scientific Computing, Cavendish Laboratory,
 Department of Physics, University of Cambridge, CB3 0HE,
 UK*

(Dated: 22 November 2017)

We present a numerical study of detonation propagation in unconfined explosive charges shaped as an annular arc (rib). Steady detonation in a straight charge propagates at constant speed but when it enters an annular section, it goes through a transition phase and eventually reaches a new steady state of constant angular velocity. This study examines the speed of the detonation wave along the annular charge during the transition phase and at steady state, as well as its dependence on the dimensions of the annulus. The system is modeled using a recently proposed diffuse-interface formulation which allows for the representation of a two-phase explosive and of an additional inert material. The explosive considered is the polymer-bonded TATB-based LX-17 and is modeled using two JWL equations of state and the Ignition and Growth reaction rate law. Results show that steady state speeds are in good agreement with experiment. In the transition phase, the evolution of outer detonation speed deviates from the exponential bounded growth function suggested by previous studies. We propose a new description of the transition phase which consists of two regimes. The first is caused by local effects at the outer edge of the annulus and leads to a dependence of outer detonation speed on angular position along the arc. The second regime is induced by effects originating from the inner edge of the annular charge and leads to the deceleration of the outer detonation until steady state is reached. The study concludes with a parametric study where the dependence of the steady state and the transition phase on the dimensions of the annulus is investigated.

Keywords: detonation propagation, annular charge, condensed-phase explosives

I. INTRODUCTION

Arbitrarily-shaped explosive charges are used in a variety of modern applications, particularly in the mining industry. The propagation of detonations in such charges is influenced by the geometry of the charge and exhibits different behavior from the case of straight charges. This study uses numerical simulations to investigate detonation propagation in unconfined annular explosive charges in air. The aim is to identify the characteristic features of detonation in such geometries and to determine its dependence on the dimensions of the annular charge.

This work is guided by two experimental studies on annular charges. The first was performed by Lyle and Hayes at the Lawrence Livermore National Laboratory (LLNL) in the 1980s and is presented in a study by Souers et al.¹. These used unconfined charges of various compositions of LX-17 shaped as a 90° annular arc with a square cross section. The detonation was initiated in a straight charge and was left to reach steady state before entering the annular section, as illustrated in figure 1. A series of electrical pins were used at the edges of the charge to measure arrival times of the detonation wave, in addition to a streak camera used to capture the shape of the detonation front. The second experiment was

^{a)}Corresponding author: ei233@cam.ac.uk

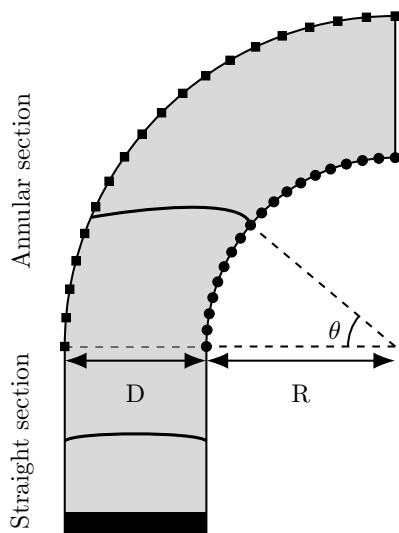


FIG. 1. Illustration of the annular charge configuration. The annulus is of width D and inner radius R . The angular position is defined by angle θ . The detonation is initiated by a booster shown as the dark region and the solid thick lines represent the detonation front. The square and circular points represent the electrical pins used to measure detonation arrival times in the Lyle experiment.

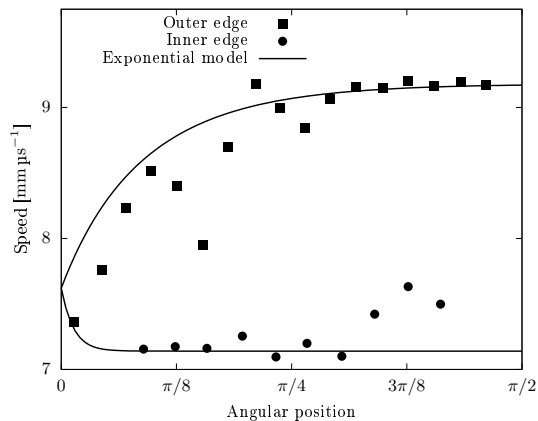


FIG. 2. Experimental measurements of detonation speeds along the outer and inner boundaries of the explosive annulus adopted from the Lyle experiment¹. The black curves correspond to the exponential model suggested by Souers et al.¹ to describe the evolution of the detonation speed along the annulus.

performed by Lubyatinsky et al.² who presented results of arrival times and front break-out traces of detonation waves propagating in 180° annular arcs of an unspecified high explosive. This experiment involved explosive annuli of various widths and radii confined by two types of material, namely steel and PMMA.

Experiments on annular charges were also performed for the purpose of calibrating and validating mathematical models for detonation propagation such as Detonation Shock Dynamics (DSD). Tonghu et al.³ studied 60°, 90° and 125° annular arcs of a TATB-based explosive. They obtained detonation arrival times and front shapes using arrays of electrical pins and high speed photography and compared them against numerical results from a DSD computational code. Similarly, Bdzil et al.⁴ measured the speed and front shape for a detonation exiting a 135° unconfined annular arc of PBX-9502. This was used for the validation of time-dependent⁵ and steady⁶ DSD calculations and were found to be in good agreement with the experimental results.

Similar experiments have been performed for gaseous explosives motivated by the development of rotating detonation engines. Nakayama et al.⁷ studied annular configurations of different inner radii and same width for a range of characteristic detonation cell width. They classified detonation propagation in different modes namely unstable, critical and stable depending on the magnitude of the variation of inner normal detonation velocity. A condition for stable propagation was determined based on the ratio of inner radius to characteristic cell width. In addition it was found that a scaled $D_n(k)$ relation exists which is almost independent of the configuration parameters, inner radius and characteristic cell width.

A common outcome of the aforementioned studies is that detonation propagation in annular charges settles to a steady state. This is characterized by constant angular velocity of the detonation wave as opposed to constant linear velocity observed in straight charges.

Furthermore, there is a dependence of the steady angular velocity on the charge dimensions, similar to the diameter effect seen in straight charges. In particular, the reciprocal steady angular velocity has an affine dependence on the inner radius of the annular arc².

The shape of the detonation front in annular charges is asymmetric, in contrast to straight charges which is symmetric about the center line. Its leading peak is close to the inner edge as seen in figure 1. Its position depends on the confining material which also affects the speed of the leading peak. Materials with high impedance induce higher leading peak speeds and smaller distances between the leading peak and the inner edge².

The condition of constant angular velocity results in notably different detonation speeds at each edge of the front. Denoting the steady detonation speed measured along the inner edge as V_S and along the outer edge as W_S , the constant angular velocity condition translates to

$$W_S = \left(1 + \frac{D}{R}\right) V_S, \quad (1)$$

where R and D are the inner radius and width of the arc respectively, as depicted in figure 1. It is evident that depending on the ratio of width to radius, steady state velocity measured along the outer edge of the charge can have a significantly larger magnitude than at the inner edge.

There is a fundamental difference in the nature of speeds measured along the inner and outer edge of the annulus. At the inner edge, the detonation front velocity is tangent to the boundary of the annular charge and the measured speed is the actual speed at which the detonation propagates along that edge. However, the detonation velocity at the outer edge is not tangent to the boundary of the annulus and does not propagate along the outer boundary. Instead, the outer edge of the detonation at any moment has originated from a previously interior part of the detonation front. Thus, the measured speed is an apparent speed that the detonation front exhibits along the curve defined by the outer boundary as if it is moving across it. This explains why the speed measured at the outer boundary can be significantly higher than the ideal CJ velocity, which would otherwise be considered nonphysical for self-propagating detonations.

The transition phase is defined as the period beginning when the detonation enters the annular section until steady state is reached. The inner part of the detonation reaches steady state earlier than the outer part which has a longer transition phase, as can be seen from the results of the Lyle experiment in figure 2.

Although the dynamics of the detonation wave during the transition phase have not been thoroughly explained, it is suggested to involve a process where equilibrium is achieved through an energy flow across the detonation front⁸. Souers et al.¹ suggest that the evolution of the inner and outer speeds during the transition to steady state follows an exponential function of time given by

$$u(t) = U_S + (u_S - U_S) \left(1 - \exp\left(\frac{-t}{\tau}\right)\right), \quad (2)$$

where u is the wave speed at either edge, u_S is the corresponding steady speed, U_S is the steady speed in the straight section and τ is a time constant. The time constant is different for the inner and outer edge and it determines the extent of the transition period. It is derived by approximating the speed of sound as three quarters of the steady detonation speed in the straight section and is given by

$$\tau = \frac{4\Delta D}{3U_S}, \quad (3)$$

where ΔD is the distance of the corresponding edge from the leading peak of the detonation front. Plots of the exponential functions that are suggested to describe the detonation front speed at the inner and outer edge of the explosive charge are shown in figure 2.

Detonations in annular charges have also been investigated by a number of numerical studies. Short et al.⁶ studied steady solutions of the DSD model for a 2D annular charge

using both numerical methods and asymptotic analysis. The results showed a multi-layer structure of the detonation and determined the dependence of angular speed and front structure on the size of the annulus and on different degrees of confinement. The analysis distinguishes between thin and thick arcs where different approximations are made for the ratio of width to inner radius. For thick arcs, the steady angular speed corresponds to the Huygens limit with correction terms which depend only on the inner confinement.

Souers et al.¹ compared results from the Lyle and Hayes experiments against numerical simulations using the LLNL production code VHEMP with program burn and the LASL-DYNA2D hydrodynamic code with the Ignition and Growth reaction rate model. The simulations were performed with a resolution of $\Delta x = 500 \mu\text{m}$ at most and show good agreement with the experimentally measured times to steady state. However, detonation speed is overestimated by VHEMP and underestimated by DYNA2D and detonation fronts have larger curvatures compared to the experimental results.

Similarly, Vágenknecht and Adamík⁹ performed three-dimensional numerical simulations of the same experiments using LS-DYNA and the beta burn model. They used a resolution of $\Delta x = 500 \mu\text{m}$ and reported good agreement with the experimental detonation front curvature parameters but they also underpredicted the steady speed values compared to the experiment. Tarver and Chidester¹⁰ used the Ignition and Growth model and a resolution of $\Delta x = 50 \mu\text{m}$ to simulate several of the aforementioned experiments on detonations in annular charges. The focus was on the steady state speeds of the detonation front for which they showed good agreement with experimental data.

The work presented here extends on the outcomes of previous studies on detonations in annular charges. It uses direct numerical simulations to present a complete description of the propagation of detonation along the annular arc. Particular focus is given to the transition phase and the identification of the effects that govern the evolution of the detonation wave during this phase.

The numerical solution is used to calculate the detonation speed along the inner and outer edge of the annular charge with respect to angular position and to time. The steady state speeds show good agreement with experimental results. However, the evolution of outer detonation speed during the transition phase deviates from the suggested exponential model. We propose a new description of the transition phase and show that it can be divided into two regimes. In the first regime, the outer detonation speed is governed by local effects at the outer boundary which lead to a dependence of detonation speed on angular position. In the second regime, effects originating from the inner boundary reach the outer edge and bring the detonation to steady state.

This work concludes with a parametric study where the inner radius and width of the annular charge are varied. This reveals the dependence of the transition phase and the steady state on the dimensions of the annular arc. We show that the reciprocal steady angular velocity has an affine relation with inner radius of the arc which was also observed by Lubyatinsky et al.². The dependence of the extent of the transition phase on the dimensions of the annular charge is studied in terms of angle and time to steady state. Both increase with width, whereas larger radii lead to a decrease of the angle at which steady state is reached. In terms of time, there is opposing behavior between configurations of small and large widths. The transition duration increases with radius for large widths but decreases for smaller widths.

The system is modeled using the recently proposed diffuse-interface method of Michael and Nikiforakis¹¹. The explosive considered is LX-17 (92.5% TATB, 7.5% Kel-F) which makes the results directly comparable to the Lyle and Hayes experiments¹. It is modeled using two JWL equations of state and the Ignition and Growth reaction rate law¹². This choice was facilitated by the existence of widely used sets of parameters for the particular explosive, as well as by the availability of accessible experimental data that can be used to validate the mathematical model and implementation of the numerical methods.

The phenomenology of the Ignition and Growth model depends on the resolution of the computations. Thus, particular care was given in ensuring that the numerical simulations are adequately resolved. This is facilitated by the use of a parallel, hierarchical, block-

structured adaptive mesh refinement framework.

This article continues with the presentation of the mathematical model in section II. The governing equations as well as the equations of state and reaction rate used to represent the explosive are described. The employed numerical methods are discussed in section III and the implementation is validated in section IV. The study of annular charges is presented in section V and a summary of the outcomes and conclusions are discussed in section VI.

II. MATHEMATICAL MODEL

Numerical simulations involving explosives under confinement require a mathematical formulation that can model the physical properties of multiple materials and capture their interactions. Modeling heterogeneous explosives, such as LX-17, poses a particular challenge because their granular aggregate micro-structure is not possible to be explicitly resolved in a mesoscale numerical simulation. Instead, it is common to use a homogenized treatment which averages the fine scale features of the explosive and accounts for the heterogeneous effects by a phenomenological reaction rate law.

The mathematical model employed in this work was proposed by Michael and Niki-forakis¹¹ and follows the approach described above. It is a hybrid formulation for interfaces between immiscible homogeneous fluids, where one of the materials is further divided into two phases following the augmented Euler approach for modeling two phase explosives. It assumes a continuum hydrodynamic representation of the materials and allows for the modeling of an explosive with distinct equations of state for the reactants and the products, and also for an additional inert material.

This formulation is particularly suitable for modeling explosives under compliant confinement because it can handle high density gradients across interfaces, without the generation of spurious oscillations in the solution. In addition, it allows for the use of most types of equations of state and can be used for both ignition and detonation propagation studies.

The mathematical model is defined by the following system of equations

$$\begin{aligned}
 \frac{\partial z \rho_1}{\partial t} + \nabla \cdot z \rho_1 \mathbf{u} &= 0, \\
 \frac{\partial (1-z) \rho_2}{\partial t} + \nabla \cdot (1-z) \rho_2 \mathbf{u} &= 0, \\
 \frac{\partial \rho \mathbf{u}}{\partial t} + \nabla \cdot (\rho \mathbf{u} \otimes \mathbf{u} + p \mathbf{I}) &= 0, \\
 \frac{\partial \rho E}{\partial t} + \nabla \cdot (\rho E + p) \mathbf{u} &= 0, \\
 \frac{\partial z}{\partial t} + \mathbf{u} \nabla z &= 0, \\
 \frac{\partial z \rho_1 \lambda}{\partial t} + \nabla \cdot z \rho_1 \lambda \mathbf{u} &= z \rho_1 \mathcal{R}.
 \end{aligned} \tag{4}$$

It features two continuity equations which represent the discrete conservation of mass for each material as well as conservation laws for the momentum and energy of the mixture. Quantities ρ_1 and ρ_2 correspond to the density of the explosive and the inert material respectively. Quantities ρ , \mathbf{u} , p and E are the mixture density, velocity, pressure and total specific energy defined as

$$E = e + \frac{\|\mathbf{u}\|^2}{2},$$

where e is the specific internal energy of the mixture.

The composition of the mixture is determined by the quantity $z \in [0, 1]$ which represents the volume fraction of the explosive and is governed by an advection equation. Equivalently, quantity $1 - z$ is the volume fraction of the inert material. The explosive material is further

divided into two phases, which represent the reactants and the products. We define $\lambda \in [0, 1]$ as the mass fraction of the reactants. This is also governed by an advection equation with a source term \mathcal{R} describing the chemical reactions that turn reactants into products. However, it is combined with the continuity equation of the explosive material and put into a conservative form which represents the conservation of mass of the reactants. The equations do not include any terms for viscous friction or heat conduction as it is assumed that their effect is negligible in this case study.

The formulation allows for the interface to diffuse on a small number of computational cells over which a set of mixture rules has to be defined. These rules relate the thermodynamic variables of the mixture to those of the individual constituents. Considering mass and energy as additive quantities, the mixture variables are given by

$$\rho = z\rho_1 + (1 - z)\rho_2, \quad (5a)$$

$$\rho e = z\rho_1 e_1 + (1 - z)\rho_2 e_2, \quad (5b)$$

where quantities with subscript 1 and 2 correspond to the explosive and the inert material respectively. Subsequently, the density and the specific internal energy of the two-phase explosive are given by

$$\frac{1}{\rho_1} = \lambda \frac{1}{\rho_a} + (1 - \lambda) \frac{1}{\rho_b}, \quad (6a)$$

$$e_1 = \lambda e_a + (1 - \lambda) e_b, \quad (6b)$$

where subscripts a and b denote quantities of the reactants and the products that comprise the explosive.

In addition to the mixture rules, the system requires closure conditions to be fully determined. Between the explosive and the inert material only one closure condition is necessary, as the density of each material is readily available from the state variables of the equations. Between the reactants and the products, two mixture rules are required as only the total explosive density is known and root finding procedures need to be followed to determine the individual reactants and products densities. Here, the closure conditions chosen are isobaric between the explosive and inert material as it has been proven to give better stability at the interfaces¹³, and isobaric and isothermal between the reactants and products as in similar studies^{14–17}. For more details on aspects of the mathematical model the reader is referred to the work by Michael and Nikiforakis¹¹.

A. Equations of state

The definition of an equation of state (EOS) for each material is required to close the system of equations of the mathematical formulation. In this work, the LX-17 reactants and products are modelled by two distinct Jones-Wilkins-Lee (JWL) equations of state and the air is modeled as a perfect gas.

The JWL equation of state can be written in the Mie-Grüneisen form

$$e - e_{\text{ref}}(\rho) = \frac{p - p_{\text{ref}}(\rho)}{\rho \Gamma(\rho)}, \quad (7)$$

$$T = \frac{e - e_{\text{ref}}(\rho)}{c_v}, \quad (8)$$

with a constant Grüneisen coefficient $\Gamma(\rho) = \Gamma_0$ and the following reference curves

$$p_{\text{ref}}(\rho) = A \exp\left(-R_1 \frac{\rho_0}{\rho}\right) + B \exp\left(-R_2 \frac{\rho_0}{\rho}\right), \quad (9)$$

$$e_{\text{ref}}(\rho) = \frac{A}{\rho_0 R_1} \exp\left(-R_1 \frac{\rho_0}{\rho}\right) + \frac{B}{\rho_0 R_2} \exp\left(-R_2 \frac{\rho_0}{\rho}\right) - Q, \quad (10)$$

where A , B , R_1 and R_2 are parameters calibrated for the particular explosive.

For the explosive products, the pressure reference curve of the JWL EOS represents the isentrope through the Chapman-Jouguet (CJ) point and is fitted to experimental data, usually from cylinder tests¹⁸. The energy reference curve is determined by integrating the pressure reference curve, since $de = -pdv$ for an isentropic process. For the reactants, the parameters are fitted to measurements of the Hugoniot locus through an initial state.

Air is modeled by the perfect gas equation of state. This can also be expressed in the Mie-Grüneisen form through the trivial reference curves

$$p_{\text{ref}} = 0, \quad (11)$$

$$e_{\text{ref}} = 0, \quad (12)$$

and Grüneisen coefficient $\Gamma = \gamma - 1$.

B. Reaction rate law

The reaction rate law used in this study is Ignition and Growth (I&G)¹² and plays an important role in capturing the reactive properties of the granular explosive within the homogeneous representation of the material. The heterogeneity of the explosive material is accounted for through this multi-stage, pressure-based reaction rate, which provides a phenomenological description of the effects of the micro-structure of the explosive using macroscopic material parameters.

The I&G reaction rate model is given by

$$\mathcal{R} = \mathcal{R}_I + \mathcal{R}_{G_1} + \mathcal{R}_{G_2}, \quad (13)$$

and the three terms are defined as,

$$\mathcal{R}_I = I(1 - \phi)^b(\rho - 1 - a)^x H(\rho/\rho_0 - 1 - \alpha) H(\phi_{\text{ig}} - \phi), \quad (14)$$

$$\mathcal{R}_{G_1} = G_1(1 - \phi)^c \phi^d p^y H(\phi_{G_1} - \phi), \quad (15)$$

$$\mathcal{R}_{G_2} = G_2(1 - \phi)^e \phi^g p^z H(\phi - \phi_{G_2}), \quad (16)$$

where $H(x)$ is the Heaviside step function, $\phi = 1 - \lambda$ is the mass fraction of the products and ρ and p are the density and pressure of the explosive respectively. The rest of the parameters are constants that are calibrated for each particular explosive.

The I&G model captures the complex ignition and burning processes in heterogeneous explosives by using three terms to represent the processes occurring in the initiation and propagation of detonations in a heterogeneous explosive¹⁵. In the shock-to-detonation transition process, ignition occurs due to shock-induced heating and friction as well as hot-spot formation through cavity collapse in porous explosives. These initiation mechanisms are represented in the ignition term (14) which is activated when density increases above a threshold α and is used only in the initial stages of the reaction.

The remaining two terms are called growth terms and have different interpretations depending on whether the application involves initiation or propagation of detonation. In the latter case, which applies to this study, the growth terms represent the formation of the products. In particular, term (15) models the rapid formation of gas products and term (16) the slow diffusion-controlled formation of solid carbon.

The JWL and I&G parameters are selected and adjusted jointly to accurately represent a specific explosive and application. For example the parameters can be different between applications that involve either ignition or propagation of detonation, even for the same explosive.

C. Data set and non-dimensionalization

The parameter sets found in the literature for the equation of state and reaction rate of a particular explosive can often vary. The variation is attributed to the different experiments

Parameters	LX-17	
	Reactants	Products
Γ_0	0.8938	0.5
A [10^{11} Pa]	778.1	14.8105
B [10^{11} Pa]	-0.050 31	0.6379
R_1	11.3	6.2
R_2	1.13	2.2
c_V [$\text{m}^2 \text{s}^{-2} \text{K}^{-1}$]	1305.5	524.9
Q [$10^6 \text{m}^2 \text{s}^{-2}$]	0	3.94
ρ_0 [kg m^{-3}]	1905	1905

TABLE I. JWL EOS parameters for LX-17¹⁶.

	\mathcal{R}_{ig}		\mathcal{R}_{G1}		\mathcal{R}_{G2}
I [s^{-1}]	4.0×10^{12}	G_1 [$\text{GPa}^{-3} \text{ms}^{-1}$]	4500	G_2 [$\text{GPa}^{-1} \text{ms}^{-1}$]	30
a	0.22	b	0.667	c	0.667
d	1	e	0.667	g	0.667
x	7	y	3	z	1
ϕ_{ig}	0.02	ϕ_{G1}	0.8	ϕ_{G2}	0.8

TABLE II. Ignition and Growth parameters for LX-17¹⁶.

to which the parameters were fitted but also to the particular process that the parameter set intends to model. The parameter data set for the explosive LX-17 used in this study is taken from the work of Tarver¹⁶ and has been used in similar studies^{15,17}. The parameters for the JWL EOS are shown in table I and the reaction rate parameters are shown in table II. This set is suggested to be more suitable for detonation propagation rather than initiation¹⁶.

The equation of state and reaction rate parameter sets are often given in a non-dimensional form, where particular parameters related to the application were used as reference values in the non-dimensionalization process. Following the example of Kapila et al.¹⁵ we use the CJ detonation speed of the explosive as one of the reference values. This is calculated analytically using the CJ theory¹⁹. The reference values used for non-dimensionalization are

$$\begin{aligned}
 \rho_0 &= \rho_{\text{ref}} = 1905 \text{ kg m}^{-3} \\
 D_{\text{CJ}} &= u_{\text{ref}} = 7.6799 \text{ mm } \mu\text{s}^{-1} \\
 t_{\text{ref}} &= 1 \mu\text{s}.
 \end{aligned}
 \tag{17}$$

From the above, the reference values for the rest of the flow variables can be calculated as

$$\begin{aligned}
 \rho_0 D_{\text{CJ}}^2 &= p_{\text{ref}} = 112.359 \text{ GPa} \\
 D_{\text{CJ}}^2 &= e_{\text{ref}} = 58.98 \text{ mm}^2 \mu\text{s}^{-2} \\
 D_{\text{CJ}} t_{\text{ref}} &= l_{\text{ref}} = 7.6799 \text{ mm}.
 \end{aligned}
 \tag{18}$$

III. NUMERICAL SOLUTION

The mathematical formulation presented in the previous section constitutes a non-linear hyperbolic system with source terms. Starting from the initial conditions, the numerical solution is advanced in time through the process of operator splitting. This allows for separate solving of the homogeneous part using an appropriate hyperbolic solver and the independent use of an ODE solver to compute the effect of the source terms.

The hyperbolic part is solved using the finite volume method MUSCL-Hancock²⁰. It is a high-resolution, shock capturing, Godunov-type reconstruction scheme which is second order accurate in time and space. To avoid the spurious oscillations near steep gradients in the flow that would otherwise occur in high order schemes, we use the van Leer slope limiter²¹ on the primitive variables. The scheme requires a Riemann solver for calculating fluxes at cell interfaces for which we use HLLC²². The non-conservative equation of the volume fraction is solved with the Godunov method for advection equations²³. The reaction rate source term, as well as geometric source terms arising from axisymmetric problems in cylindrical coordinates are solved using a 4th order Runge-Kutta method.

The model and numerical solvers are implemented within a parallel, hierarchical, block-structured adaptive mesh refinement (AMR) computational framework²⁴ which provides increased resolution at regions of interest. This allows for the computations to be performed on a highly refined grid without a high computational expense.

A. Detonation front detection

The work in this paper focuses on the analysis of the speed of a detonation wave and therefore, it requires accurate detection of the wave front and calculation of its speed. The position of the detonation front in a simulation output can only be accurate to within one grid cell at best. In addition, the use of a shock capturing numerical method means that discontinuities are smeared over a few grid cells which introduces additional uncertainty in the position of the shock.

The algorithm used in this study for detecting shock position from the numerical solution relies on the large pressure gradients across shock waves compared to the rest of the domain. After every time-step, the normalized gradient of pressure is calculated for every cell. The position and state of cells that are above a predefined threshold

$$\frac{\|\nabla p\|}{p} > 10, \quad (19)$$

are output along with the simulation time. The extracted cells are then grouped into cells that are at the same distance from the center of the annulus within a range of the cell size Δx . The positions of all cells in a group are then averaged and the calculated points mark the detonation front position. The obtained data will unavoidably have an error variance of a few computational cells but the above method provides a consistent way of detecting front location which does not depend on how the discontinuity is smeared over the cells.

The values of position over time are then used to calculate the instantaneous speed of the detonation using a central differences scheme. The calculation of derivatives from experimental or simulation data greatly increases the noise levels in them. Thus, the stencil used in this scheme is chosen to be wide, using up to ten data points in each direction in order to provide a smooth representation of the detonation front speed.

IV. VALIDATION AND GRID CONVERGENCE

The mathematical model and implementation of the numerical methods are assessed through a series of test problems to ensure their validity and suitability for the considered application. These include the study of the one-dimensional steady detonation and of the

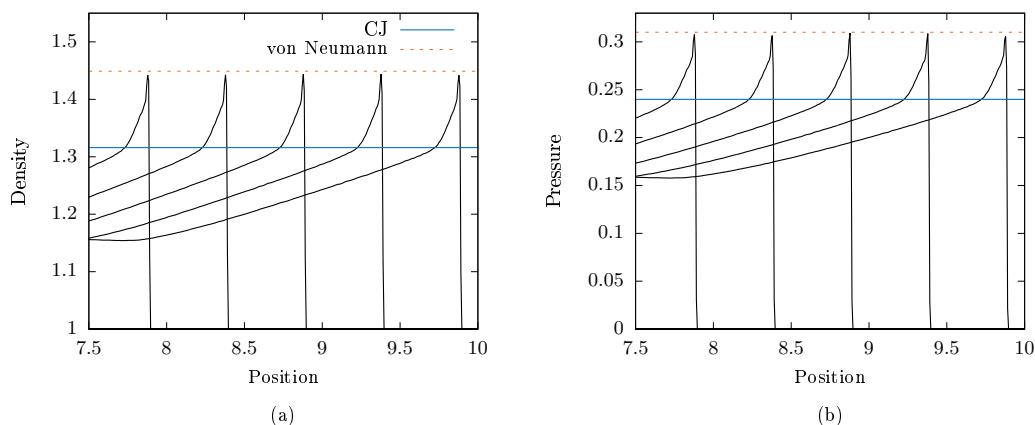


FIG. 3. The numerical solution of the one-dimensional steady detonation in LX-17. The results are plotted at constant time intervals of $t = 0.5$. The horizontal lines represent the analytically calculated values at the CJ and von Neumann points.

diameter effect in cylindrical charges. In addition, a grid convergence study is performed to establish the resolution for which the solution has sufficiently converged.

A. One-dimensional steady state detonation

We consider the numerical solution of a one-dimensional steady detonation. The structure of the detonation wave is described by the ZND detonation model¹⁹. Characteristic quantities, such as the states at the von Neumann and CJ points are calculated analytically and are used to verify the implementation of the model.

The setup is one-dimensional and contains the explosive only. The initial conditions consist of a small region of high pressure, equivalent to a booster, placed at the left end of the domain and the rest of the explosive is at ambient conditions. The pressure in the booster region is set to 0.24 (27 GPa) which is close to the expected CJ pressure of the explosive. This causes the rapid expansion of the explosive in this region, which compresses and ignites the explosive ahead, leading to the quick formation of a steady detonation wave.

The numerical solution of the one-dimensional detonation wave is shown in figure 3 for a resolution of $\Delta x = 6.25 \times 10^{-3}$. The solution is presented in a series of density and pressure plots, for times after the detonation has settled to steady state. The von Neumann and CJ points of the numerical solution match the values calculated analytically.

B. Steady detonation in cylindrical charges

The two-dimensional implementation is validated using an unconfined rate stick configuration. The setup is three-dimensional axisymmetric and is solved in a two-dimensional domain with the addition of geometric source terms. Each rate stick is defined by its radius R and has a length of $L \approx 10R$ which was found to be sufficient for the detonation to settle to steady state before it reaches the end of the charge. The detonation is initiated through a booster region of high pressure, similar to the case of the 1D steady detonation.

A base grid resolution of $\Delta x = 0.1$ is used, with two levels of refinement, each with a refinement factor of 4, yielding an effective resolution of $\Delta x = 6.25 \times 10^{-3}$. It was ensured that the solution has converged by performing a convergence study, as presented in section IVC for the case of annularly shaped charges.

The numerical solutions of steady state detonation in rate sticks of radius 10 mm and

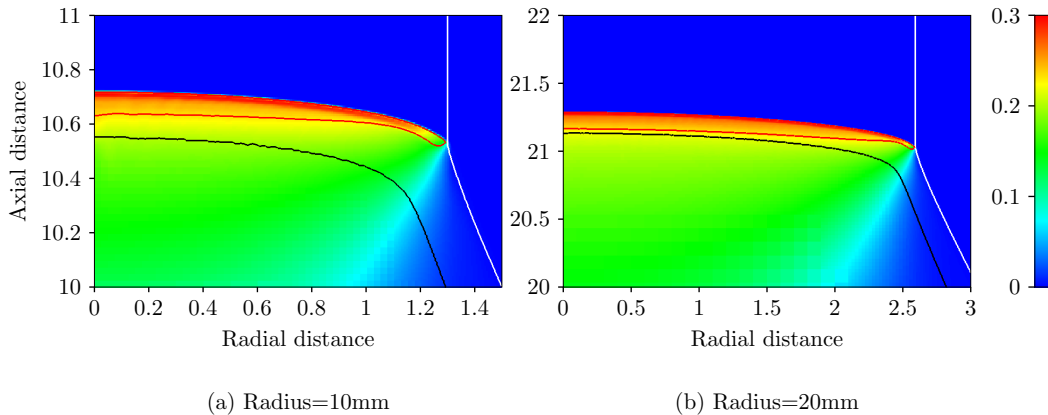


FIG. 4. Pressure plots of the structure of steady detonation waves propagating in cylindrical charges of different radii. The white line is the explosive-air interface, the black line corresponds to the reaction zone end (RZE) and the red line to the sonic locus which outlines the detonation driving zone (DDZ).

20 mm are shown in figure 4. As the detonation wave propagates, the explosive products expand against the surrounding material which results in a diverging flow as evidenced by the position of the explosive-air interface. Also depicted is the reaction zone end (RZE) locus, defined as the contour $\lambda = 0.001$ and the sonic locus, defined as the curve which satisfies

$$M \equiv \frac{\|\mathbf{v}\|}{c} = 1,$$

where \mathbf{v} is the flow velocity in the frame of the detonation and c is the local speed of sound.

The sonic locus outlines the region behind the shock in which the flow is subsonic and is often referred to as the detonation driving zone (DDZ). Outside the DDZ, the flow is supersonic and does not influence the propagation of the detonation. In the steady detonations of figure 4, the sonic locus intersects the detonation front and not the explosive-air interface. This means that the detonation wave is completely decoupled from the surrounding material because the flow along the explosive-air interface is supersonic. This classifies the configuration as unconfined, since the surrounding material has no effect on the propagation of the detonation.

The position of the sonic locus inside the reaction zone is characteristic of the diverging flow in charges of finite radius. This results in some of the chemical energy released in the reaction zone not being supplied to the detonation front. In charges of smaller radius, the curvature of the detonation front increases and the sonic locus moves further away from the RZE which results in the DDZ covering less of the reaction zone region. This translates to even less energy being used to drive the detonation wave and gives rise to the diameter effect in which the detonation slows down as the radius of the charge decreases and eventually leads to detonation failure. The difference in the position of the sonic locus with respect to the RZE for rate sticks of different radii can be seen in figure 4.

To assess the suitability of the mathematical model in capturing the dependence of detonation speed on charge radius, we compare the numerical results of detonation speeds against experimental results. The experiments were performed at the Lawrence Livermore National Lab²⁵ and used LX-17 charges confined by thin shells of either copper or PMMA, as well as bare charges. They measured the average detonation speed over the last third of the charge in which the detonation is assumed to be in steady state. The PMMA shells had thickness between 1 mm – 3.25 mm which is at most 25% of the charge radius. These configurations are considered unconfined and are used to compare against the results of the numerical simulations.

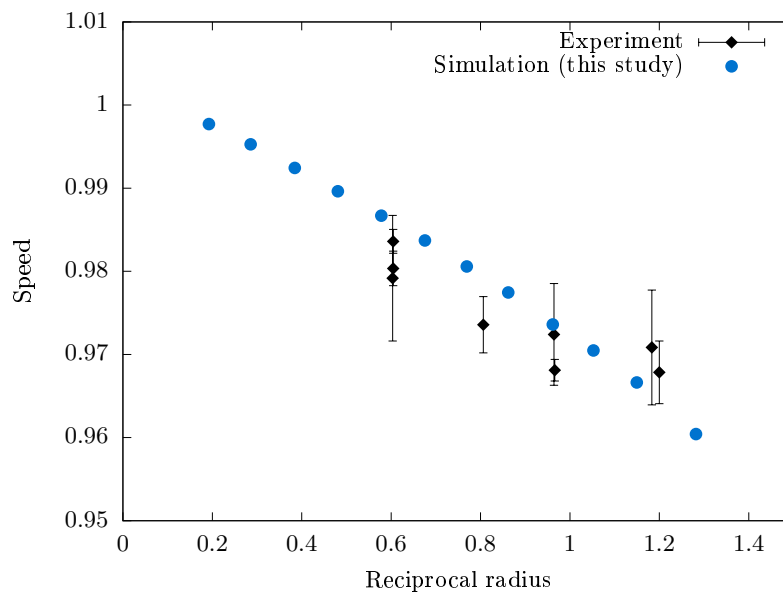


FIG. 5. Numerical and experimental²⁵ steady detonation speeds over reciprocal radius for unconfined cylindrical LX-17 charges.

The experimental and numerical detonation speeds can be seen in figure 5. The diameter effect curve obtained from the numerical solution is concave downwards which is typical of heterogeneous condensed phase explosives²⁶. The numerical detonation speeds are within the range of values of the experiment. The calculated failure radius is between 5.5 mm – 6 mm which agrees with the numerical results from Tarver and McGuire²⁷ and with their reported experimental value of 6 mm. The large error margins of the experimental values do not allow for assessing the accuracy of the numerical results. However, this test establishes the ability of the model to capture the diameter effect for condensed phase high explosives.

C. Convergence study

The use of sufficient resolution for the computations is essential in capturing the phenomenology of the Ignition and Growth model. If the reaction zone is not adequately resolved, it does not exhibit the intended phenomenological description of the reaction processes in the explosive and leads to critical loss of accuracy in the solution. Bdzil et al.⁴ studied a simplified pressure-based reaction rate law and determined that predicting the detonation speed of a straight cylindrical charge within 10 m s^{-1} of the actual value requires 50 or more cells in the reaction zone.

The convergence of the numerical solution is assessed by examining the detonation speed over time for a series of simulations of increasing resolution. We use the annular charge configuration and the detonation speed is calculated along the inner and outer parts of the charge. The domain boundary conditions are set to transmissive²² to allow for waves to exit the domain without any effect on the flow inside. This condition is not perfectly satisfied in multi-dimensional problems and partial reflections occur which influence the flow inside the domain. Thus, we ensured that the domain boundaries are sufficiently far as to not influence the reaction zone and interfere with detonation propagation.

The initial resolution is set to $\Delta x = 0.05$ which corresponds to $384 \mu\text{m}$ and is halved for every subsequent simulation. In addition, we ensure sufficient coverage of the important regions by the adaptive mesh refinement (AMR) process. This is done by comparing the

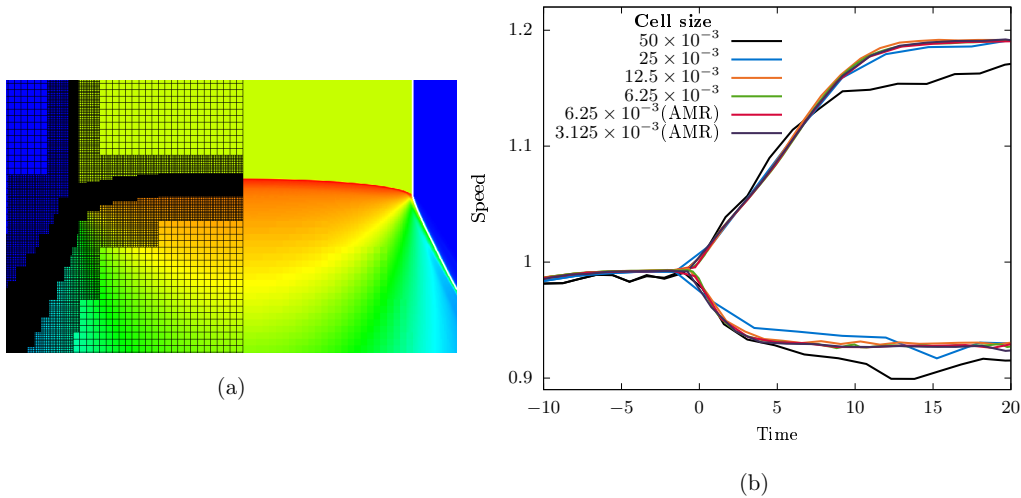


FIG. 6. Convergence and AMR coverage study for the annular arc configuration. (a) Depiction of two levels of AMR covering the detonation front and material interface. (b) Detonation speed over time at the inner and outer boundary of the explosive, calculated from solutions of increasing resolution.

numerical solution obtained using a uniform grid with one that used an AMR grid at the same effective resolution. The refinement criterion is set using the density gradient, i.e.

$$\frac{\|\nabla\rho\|}{\rho} > 1.$$

This results in refining the detonation front and the reaction zone, as well as the interface between the explosive and air due to the sharp density difference between the two materials.

Figure 6 shows the speed of the detonation wave over time at the inner and outer edge of the explosive charge for the set of resolutions used. The solution gives indistinguishable detonation speeds for resolutions higher than $\Delta x = 6.25 \times 10^{-3}$ (48 μm) which is the resolution selected for this study. Moreover, identical solutions are also obtained when utilizing AMR which ensures that the refinement criterion results in sufficient coverage of the appropriate regions.

V. DETONATION PROPAGATION IN ANNULAR ARC CHARGES

Having validated the mathematical model and the numerical algorithms we now turn to the study of the propagation of detonations in annularly shaped explosive charges. The configuration is as shown in figure 1 and consists of an unconfined explosive charge of rectangular cross section with a straight and an annular section. The annular arc extends to 90° and is defined by the inner radius R and width D . We assume that the explosive charge is sufficiently long in the direction of the axis of curvature to allow modeling the system as two-dimensional.

The explosive is ignited by the rapid expansion of a high pressure region placed at the low end of the straight charge. This leads to the quick formation of the detonation wave, which reaches steady state in the straight section and subsequently enters the annular section of the explosive charge. The detonation speed is measured along the edges of the annulus and angular position is given by angle θ , also shown in figure 1.

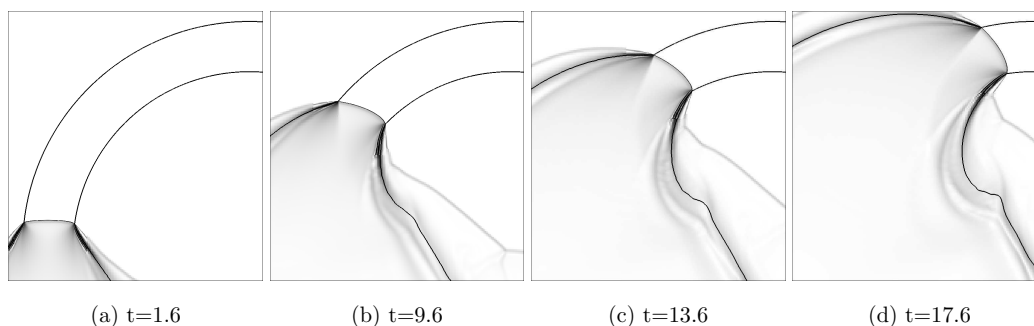


FIG. 7. Density gradient plots of the propagation of a detonation wave in an annularly shaped explosive. The dark lines represent the interface between explosive and air as well as the detonation wave front. The shock developed in the air is shown with a lighter shade. The charge is of radius $R = 11.578$ and width $D = 3.308$ which corresponds to the Lyle experiment.

A. The Lyle and Hayes experiments

We initially study the configurations used in the Lyle and Hayes experiments¹ for which experimental results are available. These used unconfined LX-17 charges of different dimensions. The Lyle experiment had an annular charge of inner radius $R = 88.9$ mm and width $D = 25.4$ mm, while the Hayes configuration had $R = 63.5$ mm and $D = 38.1$ mm. The straight section was of length $L = 116$ mm, which allowed enough travel distance for the detonation to reach steady state before entering the annular section.

Figure 7 shows density gradient plots of the detonation wave propagating in the annular section of the explosive for the case of the Lyle configuration. These plots accentuate the interface between the explosive and air as well as the detonation wave front. The shock wave in air is shown with a lighter shade. The results show the development of an apex in the explosive-air interface. This is an effect of the different geometry between the straight and annular sections. A steady detonation wave exerts a constant force on the interface in the direction normal to the interface. In the straight section this keeps the interface straight, whereas in the annular section each point of the interface is pushed at different direction and the resulting interface is curved. Thus, an apex develops at the point where the charge geometry changes.

The detonation wave is initiated and propagates steadily in the straight section at a constant speed. As it enters the annular arc every part of the front has the same linear speed and hence the outer segments have lower angular velocity compared to the inner parts. Thus, the inner parts propagate faster along the arc. This results in the deformation of the shape of the front with its peak shifted towards the inner wall. Figure 8 shows the evolution of the detonation front for the configuration of the Hayes experiment. The curvature of the detonation front shape increases during the transition period until steady state is reached, in which the front moves at constant angular velocity and maintains its shape.

Figure 9 shows the numerical results for the speed of the detonation wave along the inner and outer boundaries of the annular charge against the experimental values and the exponential time-dependent model suggested by Souers et al.¹. The inner part of the detonation moves to steady state quicker than the outer part, which has a larger transition period, consistent with the experimental results. The steady state values of the speeds are also matched well. However, the numerical results do not follow the exponential description of the transition phase. The speed at the inner edge follows a slower exponential decay than predicted by the model. At the outer edge, the detonation speed exhibits multiple stages of distinct behavior. There is a short initial period where the speed increase appears to be linear. Then the detonation exhibits increasing acceleration and eventually, the acceleration decreases until zero where the detonation has reached constant steady state speed. This behavior is notably different to the exponential model and is also within the scatter of the

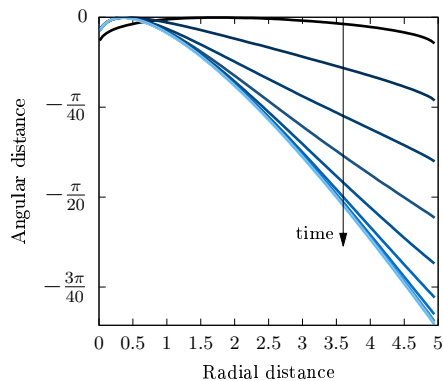


FIG. 8. Evolution of the detonation front for the Hayes configuration. The fronts are shown at constant time intervals starting when the detonation enters the annular section (black) and move from dark to light color as time progresses. The curvature of the detonation front increases until it reaches steady state and maintains its shape. Radial distance is measured from the inner edge of the charge and angular distance from the leading peak of the front.

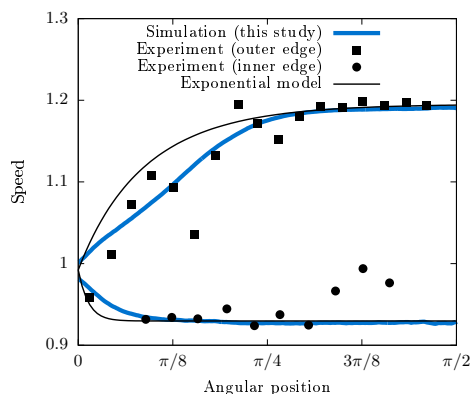


FIG. 9. Detonation speeds at the inner and outer edge of the annular charge calculated in this numerical study along with experimental results and the exponential model suggested by Souers et al.¹. The speeds are plotted against angular position θ defined in figure 1.

experimental points.

B. The effect of the boundaries of the annular charge

The study of the Lyle configuration indicated that the evolution of the detonation speed deviates from the suggested exponential model. To investigate this outcome further and understand the processes involved during the transition phase, we examine the effect of each of the two boundaries of the annular charge separately.

We consider two test cases where one of the two boundaries of the two-dimensional annular charge is removed and the remaining space is filled with the explosive. This results in a semi-infinite explosive charge with a single edge, as shown in the illustrations of figure 10. The configurations also include a straight section where the detonation is initiated and left to reach steady state. In both test cases, we calculate the speed of the detonation wave along the curve defined by the outer boundary of the original arc configuration. These curves are illustrated in figure 10 and the resulting detonation speeds for each test case are shown in figure 11.

In the case of inner-only boundary, the detonation along the outer curve initially accelerates at an increasing rate. It then reaches an inflection point and the acceleration decreases until it becomes zero and the detonation travels at constant speed. The evolution of the detonation speed in this case can be divided into two regimes based on the physical processes involved. The change of geometry at the inner edge alters the detonation dynamics and its effects travel along the front at a finite speed. The first regime corresponds to the period before the effects from the inner boundary reach the outer part of the detonation front. An inflection point signals the start of the second regime where the inner boundary effects have reached the outer part and progressively move the detonation to steady state.

During the first regime, the outer part of the detonation is yet to be affected by the changes in the geometry of the explosive charge and the change in detonation speed is a result of local effects at the curve representing the outer boundary of the original configuration.

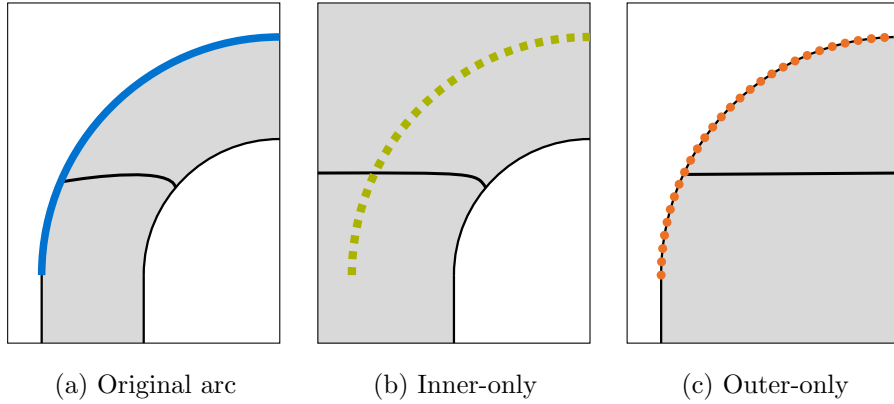


FIG. 10. Depiction of the original annular configuration and of the test cases devised to examine the influence of the boundaries of the annulus. The shaded area represents the explosive and white space is air. Detonation speed measurements are made along the curves defined by the thick lines and are pattern and color coded to match the plots of figure 11.

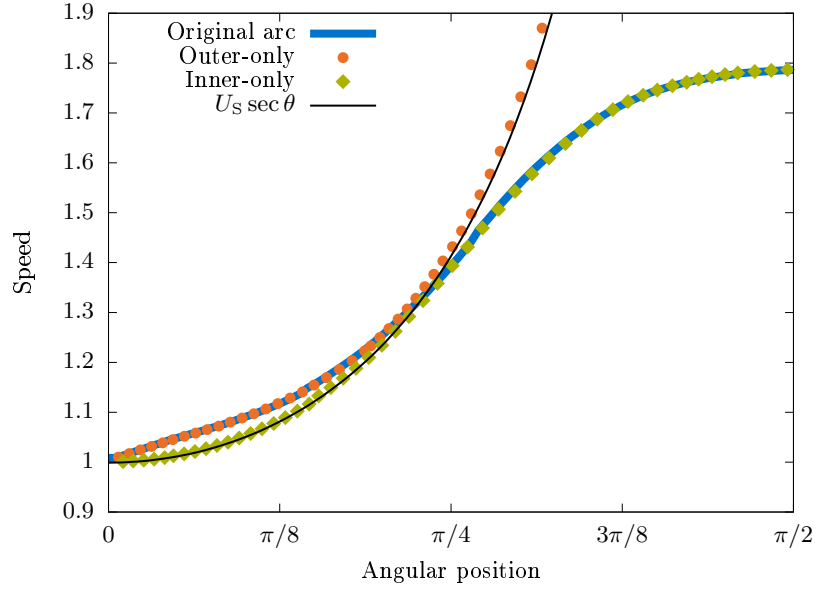


FIG. 11. Detonation speed over angular position for the devised test cases and original annular arc setup. The configuration is of radius $R = 6.616$ and width $D = 6.616$.

A mathematical description of the first regime can be deduced by considering that the detonation wave during this period is simply a plane wave propagating in the direction normal to the front. Assuming a constant straight section speed U_S , the speed measured along the curve defined by the outer boundary W will follow

$$W = U_S \sec \theta, \quad (20)$$

where θ is the angular position along the arc. Hence, the measured speed is not the actual speed at which each part of the detonation front propagates in the explosive, but rather the rate at which the detonation front reaches the curve as it travels across it.

In the second regime, the effects from the inner boundary reach the outer part causing a change in the curvature of the detonation front and in the direction of propagation. This results in the observed decrease in the acceleration of the detonation which eventually

Radius	6.616	8.27	9.924	11.578	13.232
Width	1.654	3.308	4.962	6.616	

TABLE III. The values for inner radius and width used in the parametric study to study the effect of the dimensions of the annulus

reaches steady state.

In the case of outer-only boundary, the speed exhibits an initial stage where it appears to increase linearly. This is followed by a stage of increasing acceleration of the detonation leading to very high speeds. The detonation front is flat and travels at the same direction as in the straight section.

We expect the propagation of the detonation wave in the outer-only case to be similar to the first regime of the inner-only boundary configuration because in both cases the front propagates at a constant velocity and measurements are taken along a 90° arc. Hence, the detonation speed will follow equation (20). This is indeed seen in the second stage, but with an offset, because of the observed linear increase in detonation speed during the initial stage.

The existence of the initial stage is attributed to the curvature of a small segment of the detonation front next to the outer boundary of the straight section. As discussed in section IV B the front of a steady detonation in charges of finite size is curved and its curvature depends on the diameter of the charge. In the case of outer-only boundary, the explosive charge is semi-infinite and the detonation front has a small curved segment only at the edge of the charge while the rest is flat. Due to this convex curvature, the front reaches the outer boundary faster than if it were flat, resulting in the observed linear increase. The fact that this curvature is limited to a small segment of the front next to the boundary means that only a short initial stage is influenced by it.

The detonation speed along the outer boundary for the original annular configuration is also shown in figure 11. Based on the test case of inner-only boundary, we again distinguish between two regimes in which the change in detonation speed is caused by different effects. The first regime is caused by local effects at the outer boundary of the annular charge. This leads to the behavior seen in the case of outer-only boundary, where the outer detonation speed depends on angular position; it increases linearly at first and then as $\sec\theta$. The second regime is induced by the effects of the inner edge. When these reach the outer edge of the annulus, the outer speed goes through an inflection point and the acceleration of the detonation decreases until it reaches constant steady state speed in a way that exactly follows the second regime of the inner-only test case. This shows that steady state is caused solely by the effects originating from the inner edge. Similar findings have been reported by the asymptotic analysis of a DSD model⁶. In the thick arcs approximation $D/R \sim \mathcal{O}(1)$, the dependence of steady angular velocity on inner radius and degree of inner confinement is caused by a small boundary layer region along the inner arc surface. Also, the outer radius and degree of confinement do not enter in any terms that determine the steady angular velocity.

C. The effect of the dimensions of the annular charge

The dependence of detonation propagation on the dimensions of the annular charge is investigated through a parametric study in which the width and inner radius of the annulus are varied. A set of values for the radius and width are selected as multiples of the greatest common factor of the radius and width used in the Lyle and Hayes experiments. The set of values used is shown in table III.

Simulations were performed for all twenty combinations of the values above. The obtained inner and outer speeds against angular position along the annular section are presented in

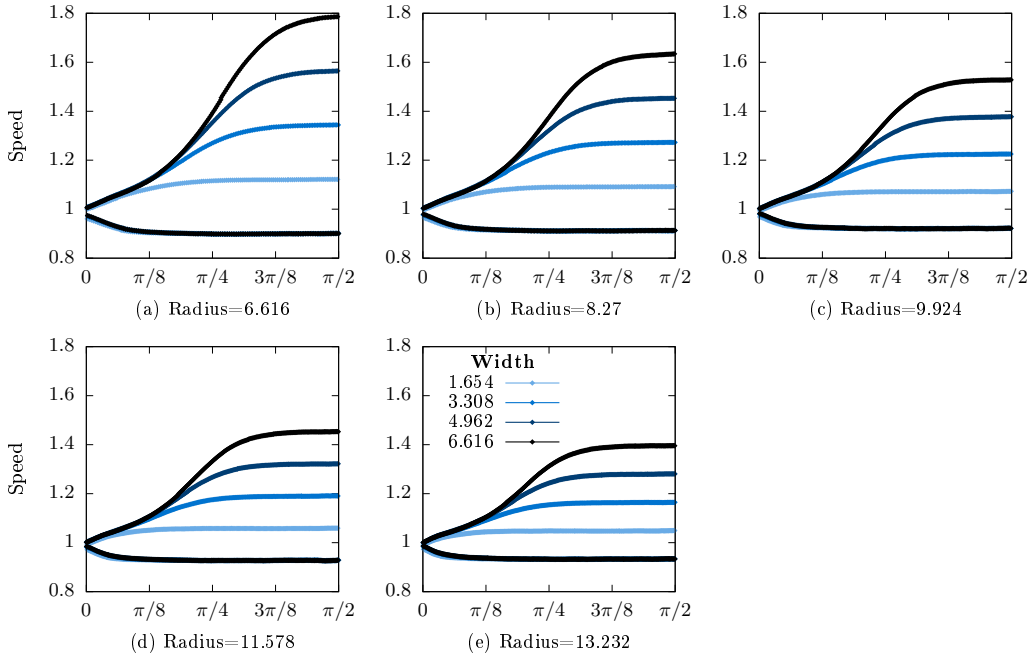


FIG. 12. Detonation speeds over angular position along the inner and outer edge of the annular arc. The plots correspond to configurations of different radii in which the width varies from small (lighter color) to large (darker color).

two sets of figures. Figure 12 arranges the results in configurations of the same radius whereas the graphs of figure 13 correspond to configurations of the same width.

We note that stable detonation was observed in all configurations. Experiments with gaseous explosives performed on similar configurations showed unsteady propagation for certain configurations. However, the minimum width employed in this study is double the failure radius of the considered explosive and any unsteady or failing detonation was not observed.

1. Steady state

We initially consider the steady state of detonation in annular arcs and investigate its dependence on the dimensions of the explosive charge. The plots of figure 12 show a clear increase of outer steady state speed W_S with width. The values are consistent with the condition of constant angular velocity given by

$$W_S = \kappa(R, D)V_S, \quad (21)$$

where V_S is inner steady state speed and κ is defined as the magnification coefficient which depends on the dimensions of the arc

$$\kappa(R, D) = 1 + \frac{D}{R}. \quad (22)$$

In contrast, inner steady speeds do not differ for explosive charges of different width and same radius. Despite the fact that steady detonation speed in the straight section increases with width due to the diameter effect, once the detonation reaches steady state in the annular section, the inner speed is the same for all configurations of the same radius. This

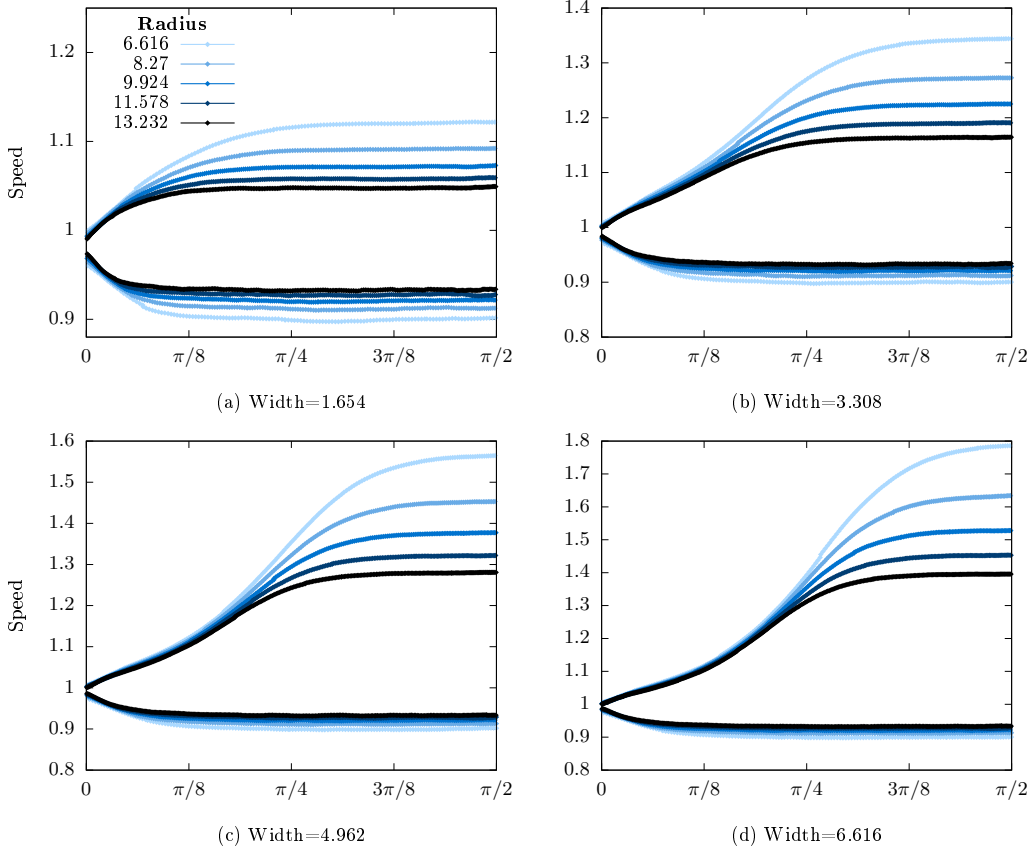


FIG. 13. Detonation speeds over angular position along the inner and outer edge of the annular arc. The plots correspond to configurations of different width, in which the radius varies from small (lighter color) to large (darker color).

implies that the steady state angular velocity, ω_S , is also independent of width since it can be expressed as

$$\omega_S \equiv \frac{V_S}{R}. \quad (23)$$

The independence of steady angular velocity on the outer radius is also seen in the asymptotic analysis of the DSD model performed by Short et al.⁶ for arcs where $D/R \sim \mathcal{O}(1)$ as in this study.

The dependence of steady angular velocity on the dimensions of the annulus is seen in figure 14. Due to the independence of the angular velocity on width, configurations of the same width fall on the same point in the plot. Furthermore, we observe an affine dependence of the reciprocal angular velocity on inner radius which agrees with the results by Lubyatinsky et al.². We perform a linear fit on the data using the model function

$$\omega_S^{-1} = \frac{R + \Delta_0}{D_\infty}, \quad (24)$$

and obtain the values

$$\begin{aligned} D_\infty &= 0.9707(11), \\ \Delta_0 &= 0.537(12), \end{aligned}$$

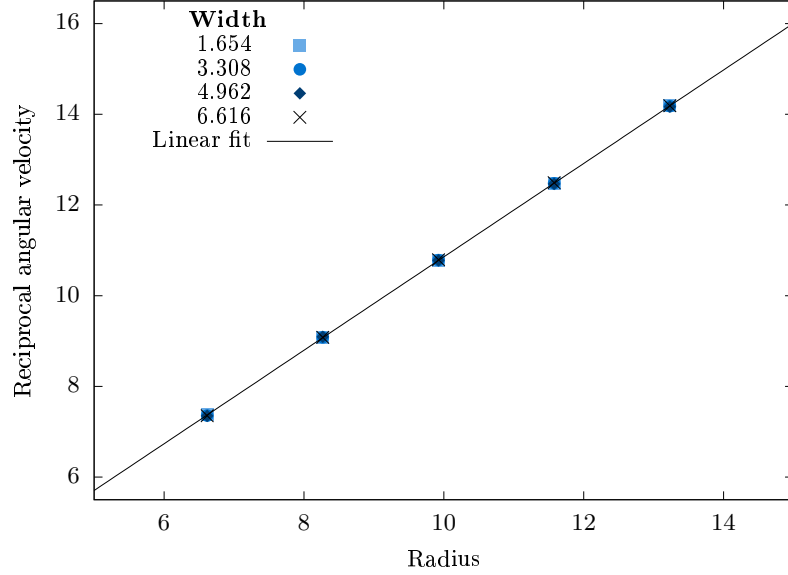


FIG. 14. The reciprocal steady state angular velocity over inner radius for all studied configurations. These show an affine dependence of the reciprocal angular velocity on the inner radius of the annulus but no dependence on the width of the annulus.

which are characteristic of the combination of explosive and confining material considered here. Parameter D_∞ represents the upper limit of detonation speed at the inner edge as $R \rightarrow \infty$. Parameter Δ_0 resembles the behavior of failure thickness of a straight explosive slab because it decreases with increasing impedance of the confining material as reported by Lubyatinsky et al.².

Expression (24) allows for the relations between inner or outer steady state speeds and the dimensions of the annulus to be determined analytically. From figure 13 we can deduce that the inner steady state speed increases with arc radius,

$$\frac{dV_S}{dR} > 0. \quad (25)$$

Utilizing equation (24), we see that the above expression holds when $\Delta_0 / D_\infty > 0$, which has to be satisfied to ensure positive angular velocity as $R \rightarrow 0$.

The dependence of the outer steady state speed on the annulus dimensions is also seen in the plots of figures 12 and 13. It increases with width

$$\frac{\partial W_S(R, D)}{\partial D} > 0, \quad (26)$$

and decreases with radius

$$\frac{\partial W_S(R, D)}{\partial R} < 0, \quad (27)$$

in contrast to the increase of steady inner speed (25). Combining relation (24) with the condition for constant angular velocity (21) shows that expression (27) holds when width is larger than a threshold,

$$D > \Delta_0. \quad (28)$$

For the explosive and confining material considered here this value is $\Delta_0 = 4.12$ mm and the condition holds for all configurations used in this study.

As expressed by (21), outer speed depends on the magnification coefficient and inner speed. These two quantities change with radius in opposite ways. The magnification coefficient decreases while the inner speed increases. Expression (28) means that when the width of the annulus is larger than a threshold, the magnification part of equation (21) is dominant and decreases more with radius than the inner speed increases, whereas the opposite applies for widths smaller than the threshold.

2. Transition phase

The transition phase is the period during which the detonation shifts from a steady state of constant linear speed in the straight section to a steady state of constant angular speed in the annular section. The inner part of the detonation front reaches steady state earlier than the outer edge of the front, which is the last segment to reach steady state speed and determines the extent of the transition phase.

The dimensions of the annulus influence the inner and outer speeds of the detonation front during the transition phase in different ways. Figure 12 indicates that configurations of different inner radius have qualitatively similar evolution of speeds whereas figure 13 shows distinct acceleration profiles of the outer detonation front for configurations of different width. In particular, configurations of larger widths demonstrate more pronounced local effects at the outer boundary and more extensive transition phases. The inner radius of the annulus only influences the last stage of the transition phase and leads to reaching steady state at smaller angles with increasing radius.

The extent of the transition phase is a function of the acceleration profile during the transition phase and of the difference between the steady speeds in the annular and straight section. Thus, its dependence on the dimensions of the annulus can be deduced from knowing the respective dependence of these two quantities. The dependence of steady speeds on the dimensions of the annulus is well understood and is presented in section VC1, but the acceleration of the outer front is only known qualitatively, as discussed in section VB and no exact function that describes the whole process is known.

We consider the extent of the transition phase in terms of angle and time. We define the equilibration angle and time as the points at which steady state is reached and thus they mark the transition phase extent. Angle is measured as shown in figure 1 and time is set to zero when the detonation wave enters the annular region. The criterion used to determine when steady state is reached is

$$W \geq 0.99W_S,$$

where W is the speed at the outer edge. The value of steady outer speed W_S , is defined in equation (21) and requires knowledge of the inner steady state speed V_S . This value is obtained from the numerical solution by averaging the speed values measured at the inner edge well after it has reached steady state.

Figure 15 presents equilibration angles and times for the studied configurations. The results indicate that both the equilibration angle and time increase with the width of the explosive annulus. Charges of larger width require more time for the effects of the inner edge to reach the outer parts which results in a more extensive transition phase in terms of both angle and time. In addition, the first regime is also more extensive and the distinctive $\sec\theta$ evolution is more prominent. In contrast, configurations of small width have a less extensive first regime and transition phase in general. In fact, for the configurations of the smallest width considered (figure 13a), steady state is reached early enough that the local effects of the outer edge do not develop significantly and the transition to steady state can be described solely by a bounded growth function.

The influence of the inner radius on the transition phase is more complex. Equilibration angle decreases with radius for all configurations but in the case of equilibration time we see opposing behavior between configurations of different width. The exponential time dependent model predicts that the transition phase duration increases with steady outer

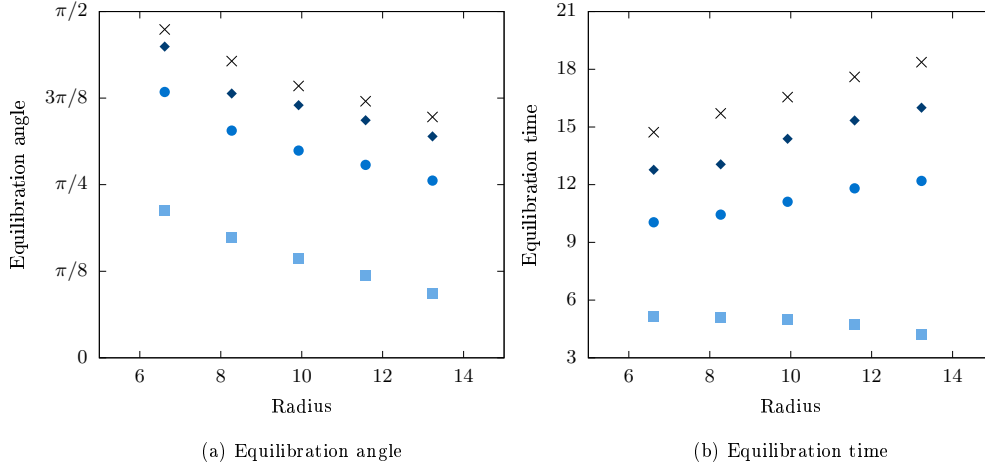


FIG. 15. Equilibration angle and time for annular arcs of different inner radius and width. Time is zero when the detonation enters the annular arc. Configurations of different width are represented as seen in the legend of figure 14.

speed. If this was a valid description of the transition phase and using expression (27), the transition phase duration should decrease with inner radius. Instead the equilibration time increases with radius, with the exception of small widths.

The increase of the transition duration despite the reduction of steady speed indicates that the acceleration of the wave front decreases with inner radius. As seen in section VB, the outer speed during the first regime of the transition phase depends on angular position which translates to a dependence on the dimensions of the annulus since,

$$\frac{dW(\theta)}{dt} = \frac{dW(\theta)}{d\theta} \frac{d\theta}{dt} = \frac{dW(\theta)}{d\theta} \frac{W}{R+D}. \quad (29)$$

The acceleration is inversely proportional to the inner radius of the annulus and hence, large radii have slower acceleration which results in reaching steady state at later times but not at larger angles. This can also be seen in figure 16, which shows detonation speeds over time during the propagation of detonation in the annular section.

The discrepancy between equilibration angles and times is a result of the local effects at the outer boundary. Thus, it is observed in configurations of sufficiently large width, where the effects of the outer edge are pronounced. If outer speed followed the suggested time-dependent exponential function during the transition phase, the transition phase duration would decrease with inner radius. This is indeed seen in small width configurations in which the local effects at the outer boundary are not developed and for which both equilibrium angle and time decrease with radius.

VI. CONCLUSIONS

This study is concerned with detonation propagation in condensed phase explosive charges consisting of a straight and an annular section. When a steady detonation in a straight charge enters the annular section, it goes through a transition phase and eventually reaches a new steady state of constant angular velocity. The characteristic features of both phases of detonation propagation in annular charges are identified and examined, as well as their dependence on the dimensions of the annular arc.

A diffuse-interface formulation¹¹ is employed for the calculations herein, which allows the modeling of a two-phase explosive with distinct equations of state for the reactant and

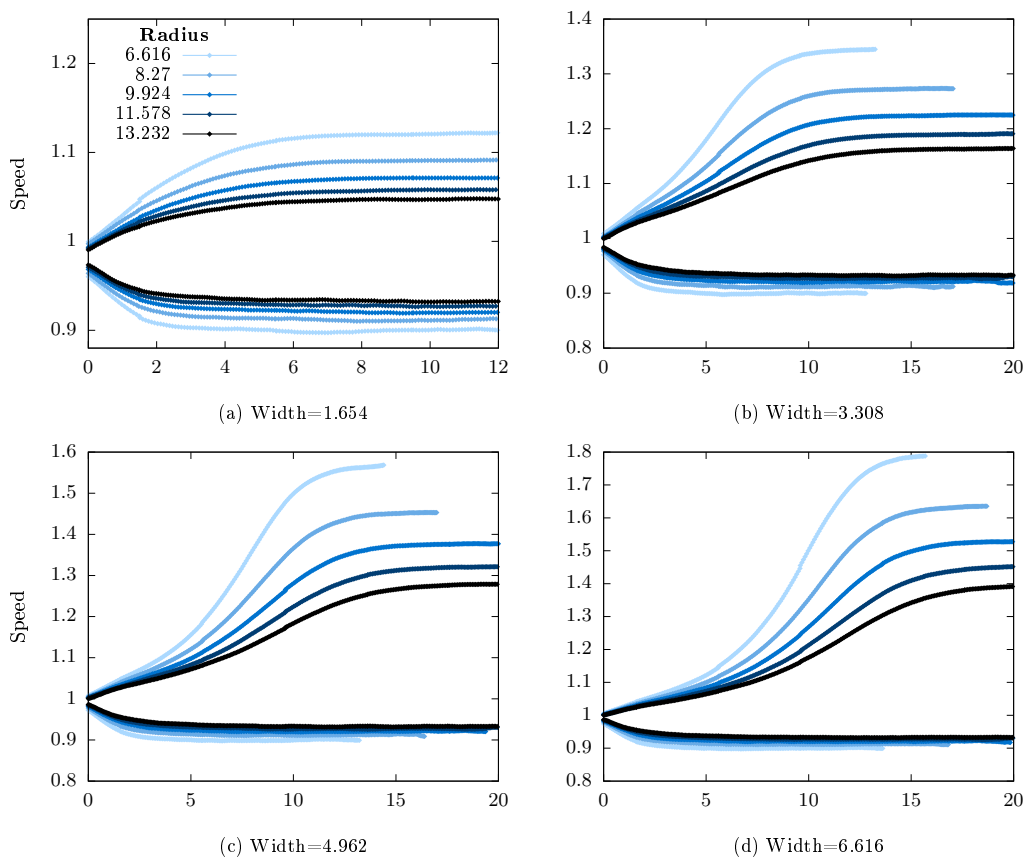


FIG. 16. Detonation speeds over time along the inner and outer edge of the 90° annular arc. The plots correspond to configurations of different width, in which the radius varies from small (lighter color) to large (darker color). Time is zero when the detonation wave enters the annular region.

products and of an additional inert material. The explosive considered is LX-17 which is a granular, porous, polymer bonded explosive. It is modeled by two JWL equations of state and the Ignition and Growth reaction rate law. This provides a macroscopic description of the effects of the micro-structure of a heterogeneous high explosive and enables the homogeneous treatment of the explosive.

The computations in this study were performed within a parallel adaptive mesh refinement framework which allows the use of high resolution with small computational cost. Convergence studies were performed for all configurations studied to ensure that the solution is independent of the grid resolution.

The mathematical model and numerical methods were validated through several tests. These included the study of steady detonation in one-dimensional and cylindrical charges. The structure of the steady detonation obtained from the numerical solution was consistent with theory and was compared against analytic solutions in the one-dimensional case. In addition, a study of detonation speed over radius in cylindrical charges was performed. This showed good agreement with experimental values and demonstrated the capability of the model to capture the diameter effect curve of the explosive.

The study of annular charges follows the configurations used in the Lyle and Hayes experiments¹. The steady state detonation speeds show good agreement with the experimental values but the transition phase deviates from the suggested exponential model. The numerical solution of the transition phase indicates that the outer speed increases linearly at the beginning, then at an increasing rate and in the final stage the acceleration decreases

to zero and the detonation reaches steady state.

The effects that govern the evolution of detonation speed during the transition phase are investigated through configurations with only one of the boundaries that make up the annular arc. These indicate that steady state is induced by effects originating from the inner edge and travel along the front at a finite speed. Thus, the transition phase of the outer speed can be divided into two regimes. In the first regime, the effects of the inner edge have not yet reached the outer part of the detonation and the outer speed is governed by local effects at the outer edge. These lead to a dependence of the detonation speed on the angular position along the arc. The second regime begins when the effects from the inner edge reach the outer part of the detonation. These change the curvature of the detonation front and lead the detonation speed towards the steady state value in a bounded growth manner.

The dependence of detonation propagation on the dimensions of the annular charge was investigated through a parametric study. We varied the inner radius and width of the charge and obtained the corresponding detonation speeds along the annulus. Results show that steady angular velocity depends only on the inner radius. In particular we observed an affine dependence of steady state angular velocity on the inner radius which has also been reported by Lubyatinsky et al.². The width of the annulus does not influence the steady angular velocity but it affects the outer steady speed which increases with width due to the condition of constant angular velocity.

The dimensions of the annulus influence the transition phase as well. The width of the charge determines the extent of the first regime of the transition phase with larger widths leading to more pronounced local effects at the outer boundary. The inner radius influences only the second regime of the transition phase. Increasing radius brings the shape of the charge closer to a straight charge and results in less difference between inner and outer steady detonation speeds, as well as reduced angles at which steady state is reached.

The extent of the transition phase was studied in terms of the angle and time at which steady state is reached. Both equilibration time and angle increase with width for configurations of the same inner radius. For annuli of the same width, increasing inner radius leads to a decrease in equilibration angle. However, the equilibration time shows different behavior depending on the width of the configuration. It increases with radius for large widths and decreases for the configuration of the smallest width.

This discrepancy is attributed to the first regime of the transition phase. The dependence of detonation outer speed on angular position during this regime leads to an inversely proportional relation between the acceleration of the outer part of the detonation and the inner radius of the annulus. This results in longer transition duration as the inner radius is increased in contrast to the decrease in equilibration angle. In the configurations of the smallest width, the equilibration time decreases with inner radius because the first regime is small and does not develop sufficiently to influence the transition duration.

ACKNOWLEDGMENTS

This work was supported by the UK Engineering and Physical Sciences Research Council (EPSRC) grant 1498435 for the University of Cambridge and by Orica Mining Services.

¹P. C. Souers, S. R. Anderson, B. Hayes, J. Lyle, E. L. Lee, S. M. McGuire, and C. M. Tarver, "Corner turning rib tests on LX-17," *Propellants Explosives Pyrotechnics* **23**, 200–207 (1998).

²V. P. Lubyatinsky, S. N. Batalov, S. V. Garmashev, A. Yu. Israelyan, V. G. Kostitsyn, O. V. Loboiko, B. G. Pashentsev, V. A. Sibilev, V. A. Smirnov, E. B. Filin, "Detonation Propagation in 180 Ribs of an Insensitive High Explosive," in *AIP Conference Proceedings*, Vol. 706, AIP Publishing (AIP, 2004) pp. 859–862.

³Z. Tonghu, L. Qingzhong, Z. Feng, H. Lishi, H. Zhi, and G. Wen, "An Experimental Study of Detonation Propagation in the Arc Insensitive High Explosive Initiated on the Basal Plane," in *Eleventh International Detonation Symposium, Snowmass, Colorado, USA* (1998) pp. 1023–1028.

⁴J. B. Bdzil, T. Aslam, T. D. Henninger, and J. J. Quirk, "High-Explosives Performance," *Los Alamos Science* **28**, 96–110 (2003).

- ⁵L. G. Hill and T. D. Aslam, “Detonation shock dynamics calibration for PBX 9502 with temperature, density, and material lot variations,” in *Fourteenth International Detonation Symposium* (2010) pp. 779–788.
- ⁶M. Short, J. J. Quirk, C. D. Meyer, and C. Chiquete, “Steady detonation propagation in a circular arc: a detonation shock dynamics model,” *Journal of Fluid Mechanics* **807**, 87–134 (2016).
- ⁷H. Nakayama, T. Moriya, J. Kasahara, A. Matsuo, Y. Sasamoto, and I. Funaki, “Stable detonation wave propagation in rectangular-cross-section curved channels,” *Combustion and flame* **159**, 859–869 (2012).
- ⁸P. C. Souers, E. McGuire, R. G. Garza, F. Roeske, and P. Vitello, “The Diverging Sphere and the Rib in Prompt Detonation,” 12th Symposium (International) on Detonation **5**, 1–7 (2002).
- ⁹J. Vágenknecht and V. Adamík, “A contribution to the analysis of corner turning rib problems,” *Propellants, Explosives, Pyrotechnics* **31**, 299–305 (2006).
- ¹⁰C. M. Tarver, S. K. Chidester, M. Elert, M. D. Furnish, R. Chau, N. Holmes, and J. Nguyen, “Ignition and growth modeling of detonating TATB cones and arcs,” in *AIP Conference Proceedings*, Vol. 955 (2008) pp. 429–432.
- ¹¹L. Michael and N. Nikiforakis, “A hybrid formulation for the numerical simulation of condensed phase explosives,” *Journal of Computational Physics* **316**, 193–217 (2016).
- ¹²E. L. Lee and C. M. Tarver, “Phenomenological model of shock initiation in heterogeneous explosives,” *Physics of Fluids* **23**, 2362 (1980).
- ¹³G. Allaire, S. Clerc, and S. Kokh, “A Five-Equation Model for the Simulation of Interfaces between Compressible Fluids,” *Journal of Computational Physics* **181**, 577–616 (2002).
- ¹⁴J. W. Banks, D. W. Schwendeman, A. K. Kapila, and W. D. Henshaw, “A high-resolution Godunov method for compressible multi-material flow on overlapping grids,” *Journal of Computational Physics* **223**, 262–297 (2007).
- ¹⁵A. K. Kapila, D. W. Schwendeman, J. B. Bdzil, and W. D. Henshaw, “A study of detonation diffraction in the ignition-and-growth model,” *Combustion Theory and Modelling* **11**, 781–822 (2007).
- ¹⁶C. M. Tarver, “Ignition and Growth Modeling of LX-17 Hockey Puck Experiments,” *Propellants, Explosives, Pyrotechnics* **30**, 109–117 (2005).
- ¹⁷C. M. Tarver, “Corner Turning and Shock Desensitization Experiments plus Numerical Modeling of Detonation Waves in the Triaminotrinitrobenzene Based Explosive LX-17,” *The Journal of Physical Chemistry A* **114**, 2727–2736 (2010).
- ¹⁸W. Fickett and W. C. Davis, *Detonation: Theory and Experiment* (Dover Publications, 1973) p. 363.
- ¹⁹J. H. Lee, *The detonation phenomenon*, Vol. 2 (Cambridge University Press Cambridge, 2008) p. 402.
- ²⁰B. Van Leer, “On the relation between the upwind-differencing schemes of godunov, engquistosher and roe,” in *Upwind and high-Resolution schemes* (Springer, 1997) pp. 33–52.
- ²¹B. van Leer, “Towards the ultimate conservative difference scheme. II. Monotonicity and conservation combined in a second-order scheme,” *Journal of Computational Physics* **14**, 361–370 (1974).
- ²²E. F. Toro, *Riemann Solvers and Numerical Methods for Fluid Dynamics* (Springer Berlin Heidelberg, Berlin, Heidelberg, 2009).
- ²³Richard Saurel, F. Petitpas, and R. A. Berry, “Simple and efficient relaxation methods for interfaces separating compressible fluids, cavitating flows and shocks in multiphase mixtures,” *Journal of Computational Physics* **228**, 1678–1712 (2009).
- ²⁴S. Schoch and N. Nikiforakis, “Numerical modelling of underwater detonation of non-ideal condensed-phase explosives,” *Physics of Fluids* **27** (2015), 10.1063/1.4905337.
- ²⁵P. C. Souers, A. Hernandez, C. Cabacungan, R. Garza, L. Lauderbach, S.-B. Liao, and P. Vitello, “Air Gaps, Size Effect, and Corner-Turning in Ambient LX-17,” *Propellants, Explosives, Pyrotechnics* **34**, 32–40 (2009).
- ²⁶S. Sheffield and R. Engelke, “Condensed-Phase Explosives: Shock Initiation and Detonation Phenomena,” in *Shock Wave Science and Technology Reference Library, Vol. 3* (Springer Berlin Heidelberg, Berlin, Heidelberg, 2009) pp. 1–64.
- ²⁷C. M. Tarver and E. M. McGuire, “Reactive flow modeling of the interaction of TATB detonation waves with inert materials,” *Twelfth International Detonation*, 1–10 (2002).